Thermal and photoinduced spin-crossover of mononuclear Fe^{II} complexes based on bppCHO ligand

*Qianqian Yang, Yin-Shan Meng, Tao Liu and Jinkui Tang**

Table S1 Crystallographic data of complex **1·ClO$_4$** at different temperature.

T/K	173	300	340	380
Formula	$C_{24}H_{18}Cl_2FeN_{10}O_{10}$	$C_{24}H_{18}Cl_2FeN_{10}O_{10}$	$C_{24}H_{18}Cl_2FeN_{10}O_{10}$	$C_{24}H_{18}Cl_2FeN_{10}O_{10}$
CCDC	2084783	2116762	2116763	2116764
Mr [g·mol^{-1}]	733.23	733.23	733.23	733.23
Crystal system	monoclinic	monoclinic	monoclinic	monoclinic
Space group	$P2_1$/c	$P2_1$/c	$P2_1$/c	$P2_1$/c
Color	Red	Red	Red	Red
a [Å]	18.4496(8)	18.5579(1)	18.5932(2)	18.6559(1)
b [Å]	8.9454(4)	9.0000(5)	9.0163(8)	9.0330(7)
c [Å]	17.2270(8)	17.3767(1)	17.4491(2)	17.5417(1)
α [°]	90	90	90	90
β [°]	94.149(3)	93.272(2)	92.848(3)	92.311(2)
γ [°]	90	90	90	90
V [Å]^3	2835.7(2)	2897.5(3)	2921.6(5)	2953.7(4)
Z	4	4	4	4
ρ_{calcd} [g·cm^{-3}]	1.717	1.681	1.667	1.649
μ[mm^{-1}]	6.689/Cu-Kα	0.781/Mo- Kα	0.774/Mo- Kα	0.766/Mo- Kα
F (000)	1488.0	1488.0	1488.0	1488.0
2θ range [°]	4.80-124.85	4.396-50.134	4.674-50.06	4.37-50.116
Reflns collected	21049	36216	37137	37423
Unique reflns	4508	5111	5153	5210
R_{int}	0.0492	0.0763	0.0869	0.1132
GOF	1.033	1.137	1.108	1.074
R_1 [I ≥ 2 σ (*I*)]	0.0381	0.0819	0.0584	0.0670
wR_2 (all data)	0.0923	0.2293	0.1860	0.2352

$$R_1 = \sum(|F_0| - |F_c|) / \sum|F_0| \quad \omega R_2 = \left[\sum \omega(|F_0| - |F_c|)^2 / \sum \omega F_0^2\right]^{1/2}$$

Table S2 Crystallographic data of complex **1·BF$_4$** at different temperature.

T/K	180	302	340
Formula	$C_{24}H_{20}B_2F_8FeN_{10}O_3$	$C_{24}H_{20}B_2F_8FeN_{10}O_3$	$C_{24}H_{20}B_2F_8FeN_{10}O_3$
CCDC	2084784	2116765	2116766
Mr [g·mol^{-1}]	725.97	725.97	725.97
Crystal system	monoclinic	monoclinic	monoclinic
Space group	$P2_1$/n	$P2_1$/n	$P2_1$/n

Color	Red	Red	Red
a [Å]	11.9099(5)	12.0228(7)	12.058(4)
b [Å]	20.2023(8)	20.1916(1)	20.187(6)
c [Å]	12.1694(4)	12.3173(6)	12.359(4)
α [°]	90	90	90
β [°]	90.8230(1)	91.178(2)	91.276(9)
γ [°]	90	90	90
V [Å]^3	2927.75(2)	2989.5(3)	3007.6(16)
Z	4	4	4
ρ_{calcd} [g·cm^{-3}]	1.647	1.613	1.603
μ(Mo-Kα) [mm^{-1}]	0.614	0.602	0.598
F (000)	1464.0	1464.0	1464.0
2θ range [°]	3.908-50.07	3.874-50.044	3.864-50.248
Reflns collected	38349	38435	38409
Unique reflns	5145	5262	5322
R_{int}	0.0741	0.0985	0.1345
GOF	1.032	1.075	1.042
R_1 [I ≥ 2 σ (I)]	0.0679	0.0687	0.0761
wR_2 (all data)	0.1868	0.2165	0.2441

$$R_1 = \sum(|F_0| - |F_c|) / \sum|F_0| \quad \omega R_2 = \left[\sum \omega(|F_0| - |F_c|)^2 / \sum \omega F_0^2\right]^{1/2}$$

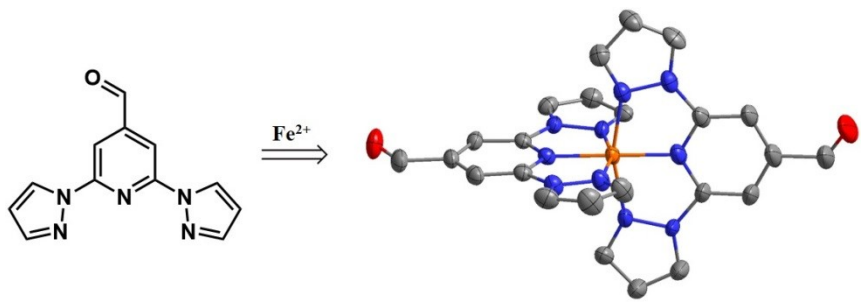

Fig. S1 Schematic diagram of crystal structure of the mononuclear Fe complexes. The probability level of atomic displacement of the ellipsoid is 30%. Color code: Fe^{II}, orange; N, blue; C, gray; O, red. The hydrogen atoms, anions, and solvent molecules have been omitted for clarity.

Table S3 Selected bond distances (Å), angles (°), and D_{2d} distortion parameters of complex **1·ClO$_4$** at different temperature.

1·ClO$_4$[173]			
Bond length (Å)			
Fe1-N1	1.979(3)	Fe1-N6	1.956(2)
Fe1-N3	1.887(2)	Fe1-N8	1.885(2)
Fe1-N5	1.959(2)	Fe1-N10	1.960(3)
Bond angle (°)			
N3-Fe1-N1	79.99(1)	N6-Fe1-N10	160.80(1)
N3-Fe1-N5	80.69(1)	N8-Fe1-N1	103.12(1)

N3-Fe1-N6	99.72(1)	N8-Fe1-N5	96.21(1)
N3-Fe1-N10	99.47(1)	N8-Fe1-N6	80.29(1)
N5-Fe1-N1	160.68(1)	N8-Fe1-N10	80.52(1)
N6-Fe1-N1	93.51(1)	N10-Fe1-N1	90.39(1)
N6-Fe1-N5	89.78(1)	N10-Fe1-N5	92.74(1)
N3-Fe1-N8 (ϕ)	176.89(1)	θ	88.45(7)
1·ClO_4^{300}			
Bond length (Å)			
Fe1-N1	1.962(4)	Fe1-N5	1.981(3)
Fe1-N2	1.958(3)	Fe1-N6	1.880(3)
Fe1-N4	1.885(3)	Fe1-N10	1.965(3)
Bond angle (º)			
N1-Fe1-N10	160.67(1)	N4-Fe1-N5	79.99(1)
N1-Fe1-N5	93.28(1)	N4-Fe1-N2	80.74(1)
N2-Fe1-N1	90.23(1)	N6-Fe1-N1	80.13(1)
N2-Fe1-N10	92.73(1)	N6-Fe1-N10	80.56(1)
N2-Fe1-N5	160.72(1)	N6-Fe1-N5	102.76(1)
N4-Fe1-N1	99.72(1)	N6-Fe1-N2	96.51(1)
N4-Fe1-N10	99.61(1)	N10-Fe1-N5	90.20(1)
N6-Fe1-N4 (ϕ)	177.25(1)	θ	88.56(9)
1·ClO_4^{340}			
Bond length (Å)			
Fe1-N1	1.963(4)	Fe1-N7	1.959(4)
Fe1-N4	1.881(4)	Fe1-N8	1.886(4)
Fe1-N5	1.984(4)	Fe1-N10	1.966(4)
Bond angle (º)			
N1-Fe1-N10	160.62(2)	N7-Fe1-N10	92.79(2)
N1-Fe1-N5	93.32(2)	N7-Fe1-N5	160.62(2)
N4-Fe1-N1	80.15(2)	N8-Fe1-N1	99.83(2)
N4-Fe1-N10	80.50(2)	N8-Fe1-N10	99.55(2)
N4-Fe1-N5	102.82(2)	N8-Fe1-N5	80.01(2)
N4-Fe1-N7	96.55(2)	N8-Fe1-N7	80.62(2)
N7-Fe1-N1	90.35(2)	N10-Fe1-N5	90.04(2)
N4-Fe1-N8 (ϕ)	177.17(2)	θ	88.55(9)
1·ClO_4^{380}			
Bond length (Å)			
Fe1-N1	1.891(5)	Fe1-N5	1.980(5)
Fe1-N2	1.967(6)	Fe1-N8	1.897(5)
Fe1-N4	1.970(6)	Fe1-N10	1.969(5)
Bond angle (º)			
N1-Fe1-N4	80.0(2)	N4-Fe1-N5	93.4(2)
N1-Fe1-N10	80.2 (2)	N8-Fe1-N4	99.9(2)
N1-Fe1-N5	103.15(2)	N8-Fe1-N10	99.9(2)
N1-Fe1-N2	96.8(2)	N8-Fe1-N5	79.9(2)

N2-Fe1-N4	90.4(2)	N8-Fe1-N2	80.1(2)
N2-Fe1-N10	92.8(2)	N10-Fe1-N4	160.1(2)
N2-Fe1-N5	160.0(2)	N10-Fe1-N5	90.3 (2)
N1-Fe1-N8 (ϕ)	176.9(2)	θ	88.60(1)

Table S4 Selected bond distances (Å), angles (º), and D_{2d} distortion parameters of complex **1·BF$_4$** at different temperature.

1·BF$_4^{180}$			
Bond length (Å)			
Fe1-N1	1.966(3)	Fe1-N6	1.960(4)
Fe1-N3	1.879(3)	Fe1-N8	1.885(3)
Fe1-N5	1.961(4)	Fe1-N10	1.961(4)
Bond angle (º)			
N3-Fe1-N1	80.55(1)	N6-Fe1-N10	161.27(1)
N3-Fe1-N5	80.72(1)	N8-Fe1-N1	100.68(2)
N3-Fe1-N6	98.99(1)	N8-Fe1-N5	98.04(2)
N3-Fe1-N10	99.74(1)	N8-Fe1-N6	80.53(1)
N5-Fe1-N1	161.25(2)	N8-Fe1-N10	80.75(1)
N6-Fe1-N1	91.89(1)	N10-Fe1-N1	91.43(1)
N6-Fe1-N5	90.09(2)	N10-Fe1-N5	92.66(2)
N3-Fe1-N8 (ϕ)	178.68(1)	θ	89.21(1)
1·BF$_4^{300}$			
Bond length (Å)			
Fe1-N1	1.960(4)	Fe1-N6	1.959(4)
Fe1-N3	1.882(4)	Fe1-N8	1.875(4)
Fe1-N5	1.961(4)	Fe1-N10	1.960(4)
Bond angle (º)			
N1-Fe1-N5	161.03(2)	N6-Fe1-N10	161.03(2)
N3-Fe1-N1	80.53(2)	N8-Fe1-N1	99.41(2)
N3-Fe1-N5	80.50(2)	N8-Fe1-N5	99.57(2)
N3-Fe1-N6	100.80(2)	N8-Fe1-N6	80.50(2)
N3-Fe1-N10	98.15(2)	N8-Fe1-N10	80.56(2)
N6-Fe1-N1	91.87(2)	N10-Fe1-N1	90.21(2)
N6-Fe1-N5	91.37(2)	N10-Fe1-N5	92.77(2)
N8-Fe1-N3 (ϕ)	178.70(2)	θ	89.25(1)
1·BF$_4^{340}$			
Bond length (Å)			
Fe1-N1	1.959(4)	Fe1-N6	1.956(5)
Fe1-N3	1.874(4)	Fe1-N8	1.884(4)
Fe1-N5	1.960(5)	Fe1-N10	1.961(5)
Bond angle (º)			
N1-Fe1-N5	160.75(2)	N6-Fe1-N1	91.94(2)
N1-Fe1-N10	91.35(2)	N6-Fe1-N5	90.1(2)
N3-Fe1-N1	80.49(2)	N6-Fe1-N10	160.97(2)

N3-Fe1-N6	99.28(2)	N8-Fe1-N1	100.81(2)
N3-Fe1-N5	80.28(2)	N8-Fe1-N6	80.69(2)
N3-Fe1-N10	99.75(2)	N8-Fe1-N5	98.41(2)
N5-Fe1-N10	92.9(2)	N8-Fe1-N10	80.29(2)
N3-Fe1-N8 (ϕ)	178.69(2)	θ	89.25(1)

Table S5 The distortion parameters (º) of complexes **1·ClO$_4$** and **1·BF$_4$** at different temperature.

	1·ClO$_4^{173}$	**1·ClO$_4^{300}$**	**1·ClO$_4^{340}$**	**1·ClO$_4^{380}$**	**1·BF$_4^{180}$**	**1·BF$_4^{300}$**	**1·BF$_4^{340}$**
Σ (º)	83.86(5)	83.63(9)	84.03(2)	86.49(9)	80.95(4)	82.01(3)	83.00(4)
Θ(º)	282.32(8)	282.02(6)	283.66(8)	290.78(3)	264.95(1)	268.93(2)	271.37(2)

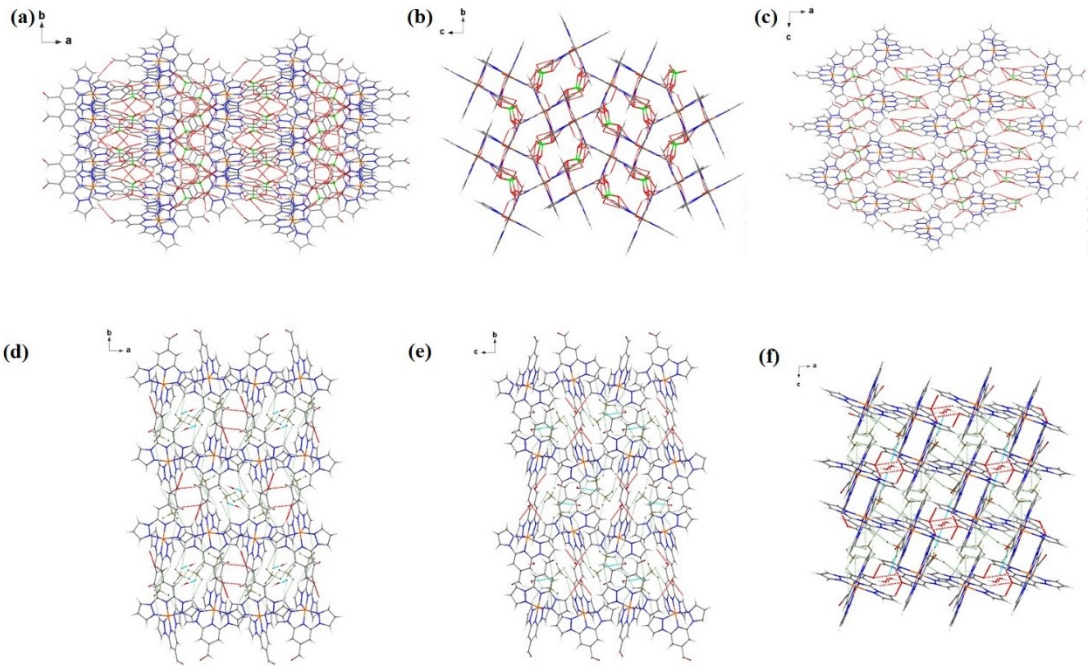

Fig. S2 Short contacts and hydrogen bonds in the packing model of complexes **1·ClO$_4$** (a, b, and c) and **1·BF$_4$**·(d, e, and f) at 173 and 180 K, respectively. Color code: Fe^{II}, orange; N, blue; C, gray; O, red; Cl, bright green; F, light green; B, dark yellow; H, white. Short contacts are represented as dashed lines: C-H···O red, C-H···F light green. Hydrogen bonds are represented as dashed lines: O-H···F turquoise.

Table S6 Interatomic distances (Å) of short contacts and hydrogen bonds for **1·ClO$_4$** and **1·BF$_4$**.

1·ClO$_4^{173}$		**1·BF$_4^{180}$**	
D—H···A	H···A / Å	D—H···A	H···A / Å
C7-H7…O1	2.462	C3-H3…O1	2.584
C12-H12…O1	2.486	C5-H5…O1	2.379
C13-H13…O1	2.373	C15-H15…O1	2.519
C23-H23…O2	2.535	C10-H10…F1	2.121
C9-H9…O3	2.378	C11-H11…F2	2.541
C3-H3…O4	2.679	C8-H8…F3	2.330
C5-H5…O4	2.594	C13-H13…F4	2.360
C23-H23…O4	2.678	C12-H12…F5	2.235

C11-H11…O5	2.551	C19-H19…F5	2.504
C15-H15…O5	2.618	C24-H24…F6	2.321
C17-H17…O5	2.481	C2-H2…F7	2.336
C21-H21…O6	2.203	C20-H20…F8	2.515
C1-H1…O7	2.460	C22-H22…F8	2.289
C19-H19…O7	2.677	O3-H3A…F2	2.153
C11-H11…O8	2.702		
C23-H23…O9	2.509		
C14-H14…O10	2.617		

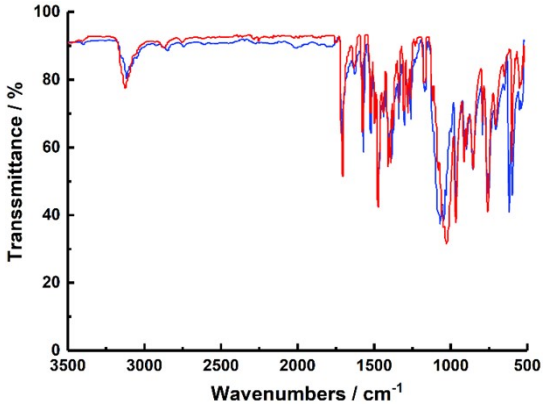

Fig. S3 IR spectra of complexes **1·ClO$_4$** (blue) and **1·BF$_4$** (red).

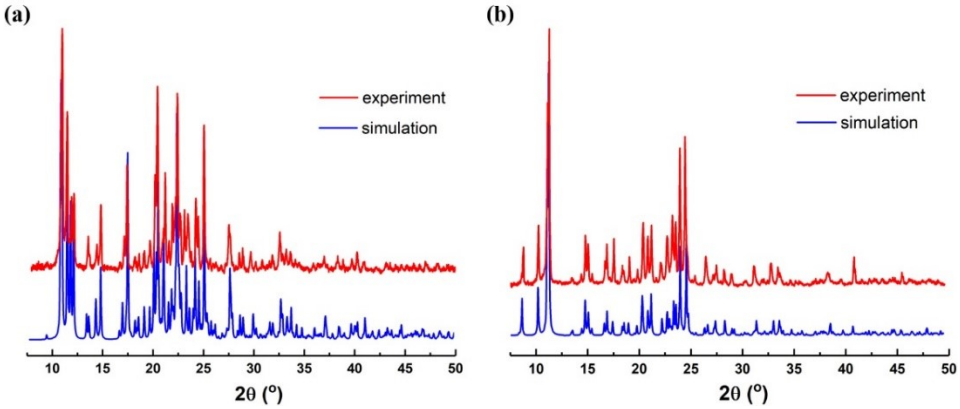

Fig. S4 Comparison between experiment and simulation of power XRD patterns of **1·ClO$_4$** (a) and **1·BF$_4$** (b) at room temperature.

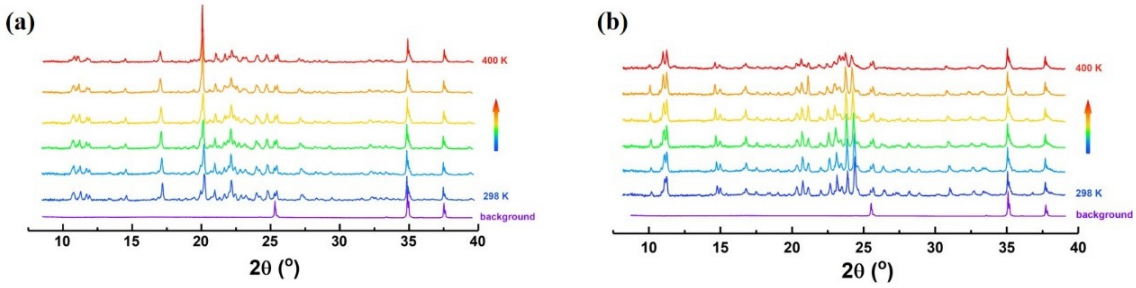

Fig. S5 Variable temperature powder XRD patterns of **1·ClO$_4$** (a) and **1·BF$_4$** (b).

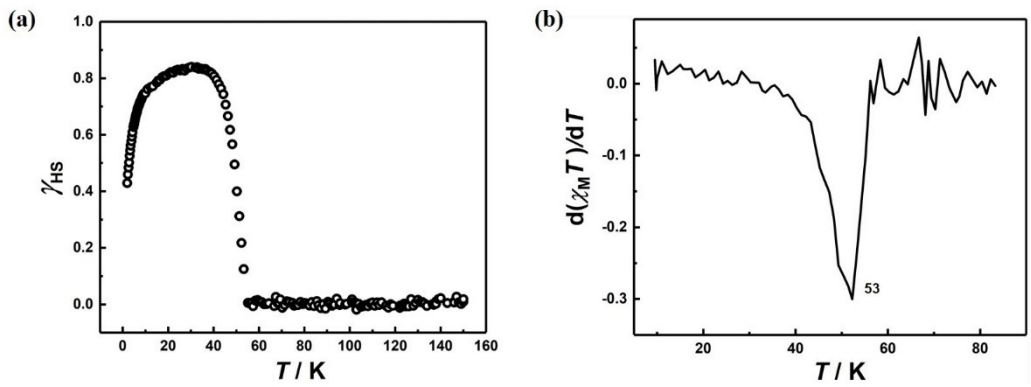

Fig. S6 (a) γ_{HS} versus *T* plot and (b) the d($\chi_M T$)/dT versus T plot of **1·ClO$_4$** after irradiation.

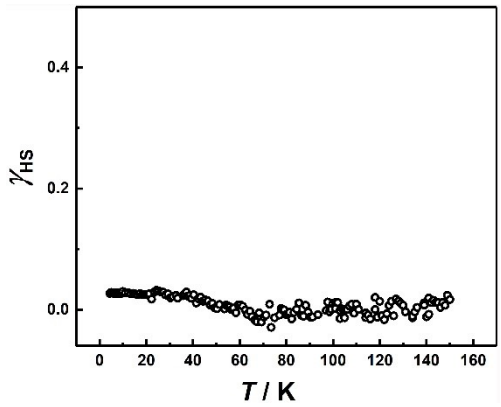

Fig. S7 γ_{HS} versus *T* plot of **1·BF$_4$** after irradiation.

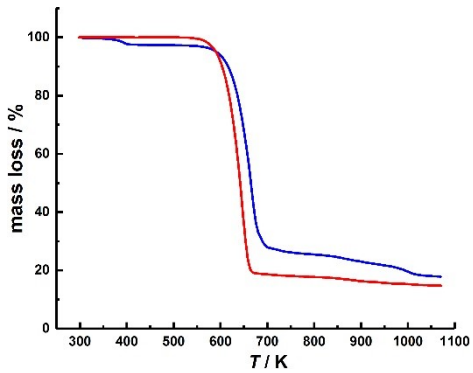

Fig. S8 Thermogravimetric profile of fresh (blue) and desolvated sample (red) of **1·BF$_4$** collected at a heating rate of 10 °C/min in N_2 atmosphere.

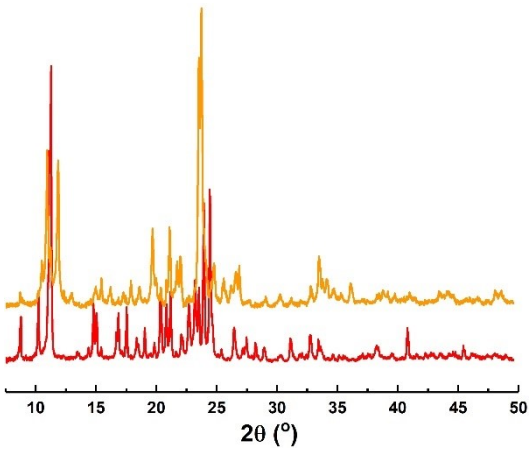

Fig. S9 Comparison between experiment of power XRD patterns of fresh (red) and desolvated sample (orange) of **1·BF$_4$** at room temperature.

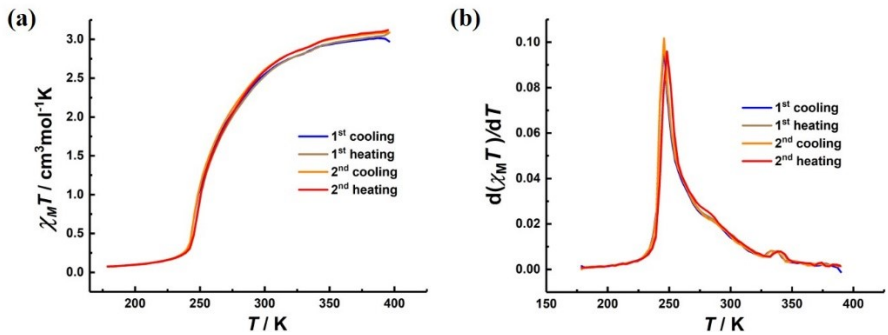

Fig. S10 (a) $\chi_M T$ vs. T plots and (b) d($\chi_M T$)/dT *vs* T plots of desolvated sample of complex **1·BF$_4$**.

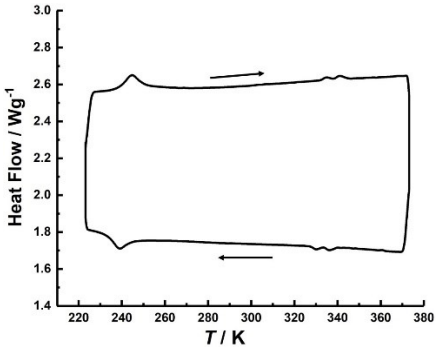

Fig. S11 DSC data for desolvated sample of **1·BF$_4$** measured by heating and cooling over -50 to 100 ˚C at 10 ˚C/min.

Table S7 The enthalpy change and entropy change of fresh and desolvated sample of **1·BF$_4$**.

		Step 1	Step 2	Step 3
Fresh sample	ΔH/ kJ mol^{-1}	1.37	0.83	2.07
	ΔS/ J mol^{-1} K^{-1}	4.01	2.49	8.34
Desolvated sample	ΔH/ kJ mol^{-1}	0.27	0.23	2.58
	ΔS/ J mol^{-1} K^{-1}	0.80	0.69	10.66